A decrease in fatty acid synthesis rescues cells with limited peptidoglycan synthesis capacity

Short title: Balancing membrane and cell wall synthesis

Jessica R. Willdigg[a] and John D. Helmann[a*]

[a]Department of Microbiology, Cornell University, Ithaca, NY, USA

[*]Address correspondence to John D. Helmann, jdh9@cornell.edu

ORCID: 0000-0002-3832-3249

Competing Interest Statement: The authors declare no conflict of interest

Keywords: cell wall, peptidoglycan, fatty acid synthesis, elongasome, antibiotic

Abstract

Proper synthesis and maintenance of a multilayered cell envelope is critical for bacterial fitness. However, whether genetic mechanisms exist to coordinate synthesis of the membrane and peptidoglycan envelope layers is unclear. In *Bacillus subtilis*, synthesis of peptidoglycan (PG) during cell elongation is mediated by an elongasome complex acting in concert with class A PBPs (aPBPs). We previously described mutant strains limited in their capacity for PG synthesis due to a loss of aPBPs and an inability to upregulate elongasome function. Growth of these PG-limited cells can be restored by suppressor mutations predicted to decrease membrane synthesis. One suppressor mutation leads to an altered function repressor, FapR*, that functions as a super-repressor and leads to decreased transcription of fatty acid synthesis genes. Consistent with fatty acid limitation mitigating cell wall homeostasis defects, inhibition of FAS by cerulenin also restored growth of PG-limited cells. Moreover, cerulenin rescued the growth of wild-type (WT) cells in the presence of otherwise inhibitory concentrations of β-lactams. These results imply that limiting PG synthesis results in impaired growth, in part, due to an imbalance of PG and cell membrane synthesis and that *B. subtilis* lacks a robust genetic mechanism to coordinate the balanced synthesis of these two envelope layers.

Importance

Understanding how a bacterium coordinates cell envelope synthesis is essential to fully appreciate how bacteria grow, divide, and resist cell envelope stresses such as β-lactam antibiotics. The balance between the peptidoglycan cell wall and the essential plasma membrane structure must be maintained for the cell to maintain shape, turgor pressure and resist external cell envelope threats. Using *Bacillus subtilis*, we show that cells deficient in peptidoglycan synthesis can be rescued by compensatory mutations which decrease the synthesis of fatty acids. Further, we show that inhibiting fatty acids synthesis with cerulenin is sufficient to reduce susceptibility to β-lactams. Understanding the coordination of cell wall and plasma membrane synthesis may provide insights relevant to antimicrobial treatment.

46 **Introduction**

47 Understanding how a bacterium coordinates the synthesis of its multiple envelope
48 components is essential to fully appreciate how bacteria grow and divide. The balanced synthesis
49 of the peptidoglycan (PG) cell wall, the cell membrane, and any additional envelope layers must
50 be maintained for the cell to maintain shape and resist turgor pressure and external cell envelope
51 threats. Many of our most powerful antibiotics target PG synthesis, and others disrupt membrane
52 synthesis or integrity. Understanding the consequences of antibiotic inhibition, and the processes
53 that ultimately lead to growth cessation or cell death, will facilitate efforts to counter the
54 emerging threat of antibiotic resistance.

55 The PG cell wall is an important structure for nearly all bacteria, allowing cells to resist
56 internal turgor pressure to prevent lysis as well as conferring shape and rigidity to the cell.
57 Seemingly contrary to its role in maintaining rigidity, the cell wall is a highly dynamic structure
58 (1, 2). The PG sacculus is constantly remodeled to accommodate the insertion of newly
59 synthesized glycan strands during cell growth and division (3). Lipid II, a lipid-linked
60 disaccharide pentapeptide PG precursor, is flipped across the cell membrane, and then the
61 glycopeptide subunits are incorporated into the sacculus by transglycosylases (TG) and
62 penicillin-binding proteins (PBPs) (4). Elongation of rod-shaped bacterial cells results from the
63 balanced action of bifunctional class A PBPs (aPBPs), which contain both TG and transpeptidase
64 (TP) activities, and an MreB-associated elongasome complex. The elongasome complex, which
65 moves circumferentially around the short axis of the cell, includes RodA (TG), class B PBPs
66 (TP), and associated endopeptidases. The aPBPs move independently and diffusely around the
67 cell during PG assembly (5-8). Although these PG synthesis machines do not move in a

coordinated manner, both aPBPs and the elongasome are necessary to maintain normal cell length and width (9, 10).

Despite recent advances, there is still much to learn about PG synthesis and assembly. *B. subtilis* has served as the premier model system for the study of envelope synthesis in Gram-positive bacteria. We have previously characterized several cell envelope stress response (CESR) pathways that facilitate adaptation to antibiotics that inhibit envelope synthesis or function (11). For example, the extracytoplasmic function (ECF) sigma factor σ^M is necessary for intrinsic resistance to PG synthesis inhibitors such as β-lactam antibiotics and moenomycin, which inhibits the TG activity of class A PBPs (12, 13). In circumstances where the aPBPs are absent due to mutation or have been inhibited by antibiotics, cells depend on the elongasome for PG synthesis. Several components of the elongasome, including RodA, are transcriptionally activated by σ^M in response to cell envelope stress (14).

An initially puzzling study revealed that cells lacking all four aPBPs (Δ4 aPBP) still synthesize PG (15), which implied the presence of an alternative TG enzyme for assembly of the glycan strands. Subsequent work revealed that RodA provides TG activity to the elongasome, and functions together with class B PBPs that provide TP activity (14, 16, 17). Previously, we used TnSeq to identify genes that become essential in cells deficient for aPBP activity (18). This led to the elucidation of a regulatory pathway that leads to the σ^I-dependent upregulation of the LytE endopeptidase and MreBH scaffolding protein (18). This pathway is initiated by the EcsA membrane protein, which is required for the function of the RasP intramembrane protease (19). RasP, in turn, cleaves multiple proteins including the anti-sigma factors for the σ^V (20, 21), σ^W (19, 22), and σ^I stress responses (23, 24). Thus, in cells lacking all four aPBPs (Δ4 aPBP), or even just the dominant enzyme PBP1 (*ponA*), the loss of *ecsA*, *rasP*, or *sigI* prevents growth on

LB medium (18). These cells fail to grow since they are unable to upregulate elongasome activity to compensate for the loss of aPBPs. Growth on LB is observed if the medium is supplemented with high levels of magnesium (Mg) ion (18), as seen also for other mutant strains with defects in PG synthesis (25). The mechanism of this suppression is unknown but may be related to a reduction of autolysin activity (25). We refer to the phenotypically similar *ecsA ponA*, *rasP ponA*, and *sigI ponA* double mutants as PG-limited strains.

Here, we took advantage of the conditional lethality of these PG-limited strains (*ecsA ponA* and *rasP ponA)* to select for growth in the absence of high magnesium. This selection revealed a cohort of suppressor mutations in genes important for fatty acid synthesis (FAS). One of these mutants, *fapR**, encodes a super-repressor that downregulates the expression of FAS enzymes. Further, we show that inhibiting FAS with cerulenin is sufficient to restore growth of PG-limited mutant strains. Characterization of the *fapR** suppressor mutation highlights the benefits of balancing membrane and PG synthesis during cell envelope biogenesis. Moreover, these genetic findings suggest that, at least in this model system, cells lack robust genetic mechanisms to coordinate membrane and PG synthesis, and that imbalanced synthesis can contribute to fitness defects.

Results

Spontaneous mutations in FAS genes compensate for lethal cell wall defects in *B. subtilis*

We selected spontaneous suppressor mutations that restore growth of strains restricted due to deficiencies in peptidoglycan (PG) synthesis (*ecsA ponA* and *rasP ponA*) in LB medium. Using this approach, we previously described three spontaneous suppressor mutations affecting the essential two-component system kinase, WalK, that affects expression of cell wall synthesis

related genes (18). Here, we report that this selection also led to mutations in several genes related to FAS. In both *ecsA ponA* and *rasP ponA* genetic backgrounds, we recovered suppressor mutations in genes encoding all four subunits of the essential enzyme acetyl-CoA carboxylase (ACC), which catalyzes the carboxylation of acetyl-CoA to malonyl-CoA, and constitutes the first committed step of FAS (26) (Table 1). We hypothesize that these mutations encode reduced function alleles of ACC that restrict the capacity for membrane biosynthesis. We also recovered both missense and deletion mutations in *fapR*, encoding the fatty acid and phospholipid synthesis repressor FapR (27). FapR responds to malonyl-CoA as an inducer to coordinate synthesis of fatty acids and phospholipids (28) .

fapR* is a dominant mutation that reduces expression of FapR-repressed genes

We focused on understanding the mechanism by which an in-frame deletion mutation, here defined as *fapR** (Figure 1A), suppressed the growth defect of PG-limited parent strains containing a *ponA* mutation in combination with either *ecsA*, *rasP*, or *sigI* (Figure 1B). The ability of *fapR** to rescue growth of all three double mutant strains is consistent with our previous data, which place *ecsA*, *rasP*, and *sigI* together in a regulatory pathway necessary for the upregulation of *lytE* and *mreBH* to support elongasome function (18). In contrast, deletion of *fapR*, which removes negative regulation on *fapR*-regulated enzymes involved in FAS, does not rescue growth of *sigI ponA* (Figure 1C). The *fapR** allele contains a 24-nucleotide deletion in the thioesterase-like domain overlapping with residue Phe99, known to be necessary for binding of the malonyl-CoA inducer (Figure 1A) (28). Thus, we hypothesized that FapR* might have reduced sensitivity to malonyl-CoA.

Further characterization of the *fapR** strain was performed to define its impact on cell physiology. Compared to WT, *fapR** strains had a significantly slower average doubling time (WT, 24 ± 0.033 min, *fapR**, 39 ± 0.11 min). The *fapR** mutant did not exhibit altered cell morphology, and no statistically significant differences in the length-to-width ratios were detected (Figure S1). Ectopic overexpression of *fapR** (but not *fapR*) resulted in a fitness defect in a merodiploid strain also containing native *fapR*, suggesting a dominant effect (Figure 1D). Collectively, these data led us to hypothesize that FapR* is a dominant super-repressor, and that rescue of strains limited in their capacity for PG synthesis can be mediated by decreased transcription of FAS enzymes.

We used qRT-PCR to directly probe the impact of FapR* on the expression levels of selected genes in the FapR regulon. In the *fapR* null strain, expression of *fabF* and *fabHA* genes was changed little (as expected, *fapR* was not detected), although the data are consistent with a modest increase. This suggests that FapR may be largely inactive as a repressor in these mid-logarithmic phase cells. In contrast, we noted a 5-10-fold decrease in the expression levels of *fabF, fabHA,* and *fapR* in the *fapR** strain (Figure 2). Mutations that eliminate the FapR-malonyl-CoA interaction are lethal, presumably because the cell is unable to sufficiently express essential FAS genes (28). We therefore hypothesized that the *fapR** allele has reduced, but not eliminated, the binding of malonyl-CoA to FapR.

FapR* is a super-repressor with reduced response to malonyl-CoA

FapR recognizes a 17-base pair operator sequence with a characteristic inverted repeat sequence (27, 28). Using the FapR operator from the *fabHA-fabF* regulatory region, we used electrophoretic mobility shift assays (EMSA) to compare the response of purified FapR and

FapR* to malonyl-CoA. When operator DNA was incubated with FapR, nearly all operator-containing fragments were shifted, whereas the control DNA fragment was unchanged. Upon titration with increasing concentrations of malonyl-CoA, the unshifted operator DNA band re-appeared (Figure 3A), suggesting that FapR is released from the DNA in response to its ligand. Conversely, DNA-binding by FapR* was relatively insensitive to malonyl-CoA (Figure 3B). With FapR, 360 μM malonyl-CoA was sufficient for release of 50% of operator DNA, whereas even >1 mM malonyl-CoA caused only a small decrease in the amount of FapR*-DNA complex (Figure 3C). This supports our hypothesis that FapR* is behaving as a super-repressor to decrease the expression of FAS enzymes, resulting in rescue of the PG-limited cells.

Addition of a membrane fluidizing agent can rescue PG-limited cells

The above results suggest that the *fapR** allele reduces membrane synthesis. However, altering the relative expression of genes in the FAS pathway could also affect membrane properties. One property known to be critical for the movement of the elongasome during PG synthesis is membrane fluidity (29). This led us to speculate that *fapR** might facilitate elongasome function by increasing membrane fluidity.

To determine whether increased membrane fluidity might be advantageous for the PG-limited *sigI ponA* double mutant, we tested the effects of the chemical fluidizing agent benzyl alcohol (BnOH). Indeed, BnOH rescued growth of *sigI ponA* at 37 ˚C on LB medium. We note that under these conditions, the *sigI ponA* strain had a high propensity for generating suppressor mutations (Figure 4A). Whole genome sequencing of selected colonies revealed mutations in *walH,* a negative effector of the essential WalK-WalR two-component system (Table S1), consistent with our previous findings where gain-of-function mutations in WalK rescue PG-

limited cells (18). However, the *rasP ponA* strain could not be rescued by BnOH under the same growth conditions (Figure 4A). It is possible that BnOH may induce other stress responses dependent on RasP. A good candidate is the RasP-dependent σ^W stress response, which increases expression of *fabF* and decreases expression of *fabHA,* thereby decreasing membrane fluidity (30). However, growth of a *sigI ponA sigW* triple mutant was still rescued by BnOH, although to a lesser extent than a *sigI ponA* strain. To test the effects of high σ^W activity on PG-limited cells, we sought to construct a *rasP ponA rsiW* strain. However, we were unable to construct this strain, which is both PG-limited and predicted to have decreased membrane fluidity (30). Thus, σ^W-dependent genes may contribute to the ability of BnOH to rescue the *sigI ponA* strain, but other RasP-dependent pathways may also be important (Figure 4B). Since both BnOH and *fapR** rescue growth of the *sigI ponA* mutant strain, it is possible that *fapR** affects both membrane synthesis and fluidity.

FapR* sensitizes cells to conditions that increase membrane fluidity

To test whether *fapR** alters membrane properties we tested sensitivity to chemical (detergent) and temperature stress. In general, cells with increased membrane fluidity often display an increased sensitivity to detergents. Indeed, the *fapR** cells were more sensitive to Triton X-100 than WT cells (Figure 5A). As noted above, detergents induce the σ^W stress response, which leads to compensatory alterations in FA composition (30). Indeed, in a *sigW fapR** double mutant, sensitivity to Triton X-100 appeared slightly higher, albeit not statistically significant, compared to the *fapR** single (Figure 5A). In a strain sensitized to heat by deletion of *sigI*, the additional presence of a *fapR** mutation increased heat sensitivity as measured by the reduced growth of the *sigI fapR** double mutant at 56 °C (Figure 5B). Consistently, introduction

of *fapR** rescued PG-limited strains (*ecsA ponA*, *rasP ponA*, and *sigI ponA*) at 37 °C, but not at 52 °C (Figure 5C), even though the *sigI ponA fapR** strain grew at 52 °C in the presence of magnesium (Figure S2). To determine the effects of the *fapR** mutation on the fatty acid constituents of the cell membrane, we performed fatty acid methyl ester (FAME) analysis. FapR* cells contained a slightly lower proportion of straight FA chains and a significant increase in the ratio of C_{17} to C_{15} acyl-chains (Table S2). It is unclear whether these changes in the FA composition of the membranes directly contribute to the apparent changes in membrane fluidity. Overall, the increased sensitivity of *fapR** to both detergents and elevated temperature supports the hypothesis that *fapR** strains have membranes with altered physical properties.

FapR* increases sensitivity to cerulenin, a FAS inhibitor

Our results suggest that *fapR** rescue of PG-limited cells is correlated with reduced expression of FAS genes. We therefore predicted that *fapR** mutants may have an increased sensitivity to cerulenin. Cerulenin is a 12-carbon mycotoxin that inhibits FAS by forming covalent linkages with β-ketoacyl-ACP synthases, including FabF, to block FA elongation (31-33). Upon inhibition by cerulenin, malonyl-CoA accumulates, triggering derepression of genes in the FapR regulon. Since FapR* is less responsive to malonyl-CoA (Figure 3), we anticipated that this compensatory mechanism might be impaired. As predicted, *fapR** mutant strains had greatly increased sensitivity to cerulenin at concentrations that did not inhibit WT or *fapR* null mutant strains (Figure 6). This effect was specific to cerulenin and unlikely to reflect general membrane permeability effects since no change was noted in sensitivity to other common hydrophobic antibiotics (Figure S3). Interestingly, *fapR** also did not affect sensitivity to triclosan (Figure 6),

227 an antibiotic which inhibits the second reduction step of FAS and, like cerulenin, normally
228 triggers induction of the *fapR* regulon (34).
229
230 **Chemical inhibition of FAS is sufficient to rescue PG-limited *rasP ponA* cells**
231 Since *fapR** rescues growth of PG-limited strains by restricting FAS, we hypothesized
232 that antibiotics that inhibit FAS might also rescue growth. Remarkably, cerulenin rescued growth
233 of the PG-limited *rasP ponA* strain (Figure 7). With optimal concentrations of cerulenin (1.65 or
234 3.3 μg mL^{-1}), growth was comparable to that of the magnesium supplemented medium (Figure
235 7). Cerulenin can also lead to a reduction in protein synthesis similar to that experienced
236 following nutrient deprivation (35, 36). However, PG-limited cells could not be rescued by
237 treatment with sub-MIC levels of the protein synthesis inhibiter chloramphenicol (Figure S4A),
238 or by reducing growth rate through non-preferred carbon sources (Figure S4B). Previously, cells
239 lacking (p)ppGpp were found to be more sensitive to cerulenin (37). However, in our strains the
240 effect of *fapR** appear to be independent of (p)ppGpp synthesis. Specifically, a *sigI* strain is
241 sensitive to cefuroxime (CEF), which inactivates PBP1, and this sensitivity is suppressed by
242 *fapR** in both *sigI* and *sigI* (p)ppGpp null strains (Figure S4C).
243
244 **Cerulenin is antagonistic with selected PG synthesis inhibitors**
245 We reasoned that if restriction of FAS by cerulenin rescues strains that are PG-limited
246 due to mutations (*rasP ponA*), it might also reduce sensitivity to PG-targeting antibiotics. To
247 determine if cerulenin affects sensitivity to antibiotics that target PG synthesis we used a
248 checkerboard assay. When WT *B. subtilis* was treated with cerulenin and CEF, we observed a
249 fractional inhibitory concentration index (FICI) of 2.5 (Table 2), indicating an additive effect.

However, in a *sigI* mutant (which is more CEF sensitive than WT), we observed strong cerulenin-CEF antagonism (FICI of 16) (Table 2). Further, treatment of WT cells with low doses of cerulenin inhibits the characteristic CEF-induced lysis evident as a loss in optical density (Figure S5). We conclude that antibiotics that inhibit FAS (cerulenin) and cell wall synthesis (CEF) display an antagonistic interaction in the *sigI* mutant. We next tested a variety of antibiotics targeting different steps in PG synthesis, including fosfomycin (UDP-GlcNAc-enoyl pyruvate synthesis), D-cycloserine (D-Ala-D-Ala synthesis), bacitracin (undecaprenyl-pyrophosphate recycling), and nisin and vancomycin (lipid II binding and sequestration). Of these compounds, only cerulenin and bacitracin displayed an antagonistic relationship (Table 2), We conclude that inhibition of FAS can reduce the efficacy of antibiotics that affect membrane-localized steps in PG synthesis.

Discussion

All cells are defined by a membrane, a boundary layer comprised largely of lipids and proteins. In Bacteria, the cell membrane is rich in phospholipids and houses numerous proteins involved in transport of nutrients and ions, energy generation, and cell signaling. The membrane is supported by the peptidoglycan cell wall, a covalently crosslinked meshwork that provides structural stability and shape to the cell. In many Bacteria, additional layers may also be present including the lipopolysaccharide-containing outer membrane in Gram-negative bacteria, S-layers, or mycomembranes. Collectively, the resulting multilayered structure is defined as the cell envelope.

Considerable progress has been made in defining how synthesis of each individual envelope layer is regulated. For example, *in B. subtilis,* FAS and phospholipid synthesis are

273 coordinated in response to malonyl-CoA precursor availability by the FapR repressor. Depletion
274 of the fatty acyl-phosphate synthase, PlsX, halts both FAS and phospholipid synthesis, which
275 suggests that *plsX* also plays a key regulatory role in coordinating FAS and phospholipid
276 synthesis (38, 39). Similarly, PG synthesis is homeostatically regulated by multiple mechanisms
277 that control the GlmS-dependent partition of fructose 6-phosphate into amino sugar synthesis.
278 GlmS expression is feedback regulated by a GlcNAc-sensing riboswitch, and UDP-GlcNAc
279 negatively regulates the activity of GlmR, an activator of GlmS activity (40, 41). In Gram-
280 negative bacteria, stabilization or degradation of LpxC, the rate-limiting enzyme for
281 lipopolysaccharide (LPS) biogenesis, fine-tunes LPS synthesis in response to situational demand
282 (42). For example, phospholipids mislocalized to the outer leaflet of the outer membrane are
283 degraded by the phospholipase, PldA, and the resulting fatty acyl-CoA molecules inhibit LpxC
284 degradation and increase LPS synthesis (43). While these mechanisms regulate individual
285 structures within the cell envelope, it is presently unclear if or how bacteria coordinate the
286 synthesis of the various cell envelope layers with each other.

287 Synthesis of the individual cell envelope layers must be uncoupled under some
288 conditions. For example, L-forms are able to synthesize membranes even in the absence of PG
289 (44-46), and photosynthetic Bacteria can synthesize abundant internal membranes without a
290 coordinate increase in PG synthesis (47). In *E. coli*, FAS has been implicated as a main
291 determinant of cell size (36). Spontaneous suppressor mutations in *fabH* can compensate for
292 lethal defects in LPS synthesis, and also reduce the rate of cell envelope growth (48). Further, *B.*
293 *subtilis* supplemented with exogenous fatty acids will increase in size by up to 10 percent,
294 suggesting that increased membrane synthesis can allow increased cell wall synthesis (36).

Here, we sought to better understand the stresses associated with a genetically-imposed, limited capacity for PG synthesis. As shown previously, cells lacking all four aPBPS (Δ4 aPBP) or even just the dominant aPBP (*ponA*) are viable on LB medium only because stress responses increase the synthetic capacity of the elongasome. The activation of σ^M increases expression of the RodA TG, as well as other PG synthesis enzymes, and a *ponA sigM* double mutant is inviable (14). Similarly, σ^I is required in a *ponA* null mutant to increase elongasome activity by increasing expression of elongasome-associated MreBH and LytE proteins (18).

Using forward genetics, we selected for suppressors of PG-limited strains lacking the major aPBP (*ponA* mutation) and defective in the σ^I pathway (e.g. *ecsA, rasP* or *sigI* mutants). One mechanism of rescue involves the up-regulation of the essential WalK-WalR two-component system through either gain-of-function mutations in WalK (18) or mutations affecting the negative regulator WalH (Table S1). Here, we demonstrate that this growth restriction can also be rescued by mutations affecting FAS. We recovered missense mutations that we hypothesize decrease ACC activity. However, efforts to further explore these mutations were frustrated by our inability to introduce these mutations into WT cells. This hints that an insufficient capacity for FAS is not well tolerated in cells with normal PG synthesis capacity. YqhY has been implicated as a possible negative regulator of ACC (49, 50). However, induction of *yqhY* did not rescue our PG-limited strains, suggesting that simply overexpressing YqhY may not be sufficient to downregulate ACC activity.

We focused our attention on *fapR**, an allele that decreases expression of FAS genes and restores growth on LB medium. The genetic rescue we observe is likely due to a decrease in membrane synthesis. Indeed, reducing FAS activity with cerulenin can also rescue growth (Figure 7). Our phenotypic analysis suggests that the *fapR** allele may also alter membrane

properties. Membrane fluidity is important for elongasome-dependent PG-synthesis (51-53), and the *fapR** allele increases sensitivity to both detergents and temperature. These phenotypes are suggestive of a possible fluidizing effect on the membrane. Further, a membrane-fluidizing agent can also rescue growth of the PG-limited *sigI ponA* strain (Figure 4). Taken together, the decrease in expression of FAS genes, possibly in conjunction with altered membrane properties, enables the *fapR** allele to restore growth of PG-limited cells. There is currently no known mechanism in *B. subtilis* to coordinate FAS with PG assembly. In the absence of such a regulatory mechanism, antibiotics can perturb balanced synthesis and thereby create an opportunity for spontaneous suppressors to develop, such as *fapR**, that re-balance FAS with PG synthesis.

Collectively, our results suggest that ongoing membrane synthesis in PG-limited cells contributes to cell death, and that cells lack a robust mechanism to slow membrane production when PG synthesis is restricted. These findings highlight the importance of maintaining a balance between membrane and PG synthesis. A more complete understanding of the balance between FAS and cell wall synthesis can provide further insights relevant to antimicrobial treatments and the maintenance of cell homeostasis.

Materials and Methods

Growth conditions, bacterial strains, and plasmids

All strains were cultured in lysogeny broth (LB) medium at 37 °C and aerated on an orbital shaker at 300 RPM. Glycerol stocks were streaked on LB agar plates and grown overnight at 37 °C. When needed, antibiotics were used in growth media at the following concentrations: 100 µg/mL ampicillin; 10 µg/mL chloramphenicol; mls (1 µg/mL erythromycin plus 2.5 µg/mL

lincomycin); 10 µg/mL kanamycin; 100 µg/mL spectinomycin, 10 µg/mL tetracycline. All synthetic lethal strains were grown in media supplemented with 20 mM $MgSO_4$. Bacterial strains used in this study are listed in supplemental Table S3. Deletion strains were created by utilizing the BKK/BKE genomic knockout library available at the Bacillus Genome Stock Center (BGSC). Gene deletions with kanamycin or erythromycin cassettes were moved into the lab WT 168 strain, taking advantage of the natural competence of *B. subtilis* grown to OD_{600nm} 0.8 in modified competence (MC) media. Null gene mutations were created by removing the antibiotic resistance cassette to create a clean in-frame null mutation using pDR244 as previously described (Koo et al., 2017). Null mutations were confirmed via colony PCR using the designated check primers as detailed in Table S4. For strains with low levels of natural competence, SPP1 transfection was used to create mutations as preciously described (54). The FapR* suppressor mutations were reconstructed via CRISPR-cas9 mutagenesis using the pJOE8999 as described previously (55). Primer sequences for repair template, guide RNA and construct confirmation can be found in Table S4. Constructs produced via CRISPR-cas9 mutagenesis were confirmed via Sanger sequencing performed by the Cornell University Biotechnology Resource Center (BRC). Genes were expressed ectopically at the *amyE* locus using the pPL82 plasmid (56) and expressed from a $P_{spac(hy)}$ promoter after induction with 1 mM IPTG.

Plating efficiency

All strains were grown in 5 mL LB supplemented with 20 mM $MgSO_4$ at 37 °C with shaking until OD_{600nm} ~0.4-0.5. The cells were washed by centrifuging 1 mL of culture at 5000 RPM, and the pellet was resuspended in 1 mL LB without additional magnesium. Serial dilutions were

364 performed and 10 µL of culture was spotted onto an LB-agar plate, air dried for 15 minutes and
365 then incubated overnight at 37 °C. N=3. A representative image is shown.
366
367 **Growth assay**
368 From a colony, strains were grown in 5 mL LB medium supplemented with 20 mM $MgSO_4$ at 37
369 °C with shaking until OD_{600nm} ~0.4-0.5. The cells were washed by centrifuging 1 mL of culture
370 at 5000 RPM, and the pellet was resuspended in 1 mL LB medium to remove traces of $MgSO_4$ or
371 resuspended in minimal media (15 mM $(NH_4)2SO_4$, 0.8 mM $MgSO_4$ $7H_2O$, 3.4 mM sodium
372 citrate dihydrate, 2 mM KPO_4, 4.2 mM potassium glutamate, 40 mM morpholinepropanesulfonic
373 acid (MOPS), pH 7.4, 0.25 mM Tryptophan, 5 µM $FeSO_4$, 5 µM $MnCl_2$, 2 % carbon as
374 specified) as required. 1 µL of this culture was added to 199 µL of media with the desired drug
375 concentration into the well of a 100-well Honeycomb plate (Steri). The OD_{600nm} of each well was
376 measured at 37 °C with shaking in a Bioscreen C growth curve analyzer (Growth Curves USA,
377 NJ) every 15 minutes up to a maximum time of 24 hours. All data shown is representative plots
378 and standard deviations from three biological replicates.
379
380 **Disc diffusion assay**
381 Cultures were grown in LB medium at 37 °C with aeration and synthetic lethal cultures were
382 supplemented with 20 mM $MgSO_4$. Cells were harvested at ~0.4 OD_{600nm}, and where applicable,
383 pelleted and resuspended in fresh LB medium to remove traces of $MgSO_4$. 100 µL of the liquid
384 culture was added to 4 mL of top agar (0.75 % agar) maintained at 50 °C to prevent
385 solidification. After mixing, top agar and cells were poured onto a 15 mL agar plate (1.5 % agar)
386 and allowed to solidify. Top agar was allowed to dry for 15 minutes prior to placing a 6 mm

387 diameter Whatman paper filter disc on the surface of the top agar. The compound of interest was
388 them immediately applied to the filter disc and the plates were incubated overnight at 37 °C. The
389 diameter of the zone of inhibition or the diameter of the zone of growth were measured and
390 recorded. Compounds were used at the following concentrations: 10 µL of a 25 % solution
391 Triton X-100, 10 µL of a 10 % solution benzyl alcohol (BnOH), 10 µg cerulenin, 5 µg triclosan
392 unless otherwise specified, 0.8 µg erythromycin, 8 µg chloramphenicol, 10 µg cefuroxime.
393

394 **Transcript analysis (Real-time RT-PCR)**

395 To determine gene expression via RT-PCR, strains were grown in LB medium to ~OD_{600nm} 0.4.
396 To extract RNA, 1.5 mL of cells were incubated at 37 °C for 15 minutes in lysozyme-TE (30
397 mM Tris-HCl, 1 mM EDTA; pH 8.0 with 15 mg/mL lysozyme) to mediate cell lysis. RNA was
398 purified as per the manufacturer's instructions using the Qiagen RNeasy Kit. The extracted RNA
399 was DNase treated according to the Turbo DNase kit manufacturer's instructions (Ambion). 2 µg
400 of RNA was used in a 20 µL reaction to synthesize 100 ng/µL of cDNA using the Applied
401 Biosystems high-capacity reverse transcription kit. Gene expression was measured using 100 ng
402 of cDNA and 0.5 µM of gene specific primer (see Table S4) and 1x SYBR (Bio-Rad) in a qPCR
403 QuantStudio 7 Pro (ThermoFischer Scientific). *gyrA* was used as a house-keeping gene. Gene
404 expression was normalized to *gyrA* and then expression values ($2^{-\Delta ct}$) were recorded for each
405 gene.
406

407 **Purification of FapR and FapR***

408 *E. coli* BL21 DE3 cells were freshly transformed with a pET-16b expression vector containing
409 an IPTG inducible copy of *fapR* or *fapR** with an N-terminal 10x-His tag. Transformants were

410 grown overnight in LB medium supplemented with ampicillin as specified and 1 % glucose. The
411 next day 100 µL of the overnight culture was used to inoculate a 3 mL pre-culture of LB medium
412 with 1 % glucose and ampicillin. The pre-culture was used to inoculate 500 mL of LB medium
413 with 1 % glucose and ampicillin and allowed to grow until ~0.2 OD_{600nm}. Cultures were induced
414 with 1 mM IPTG and additional ampicillin and left at 37 °C for 3 hours. Cultures were spun
415 down in a chilled rotor at 3500 RPM for 20 minutes at 4 °C and pellets were stored at -80 °C
416 until purification. Cells pellets were resuspended in 5 mL chilled resuspension buffer (20 mM
417 Tris-HCl, 500 M NaCl, 10 mM Imidazole, 0.5 tablet of cOmplete Mini protease inhibitor
418 cocktail (Roche), pH 7.4). Cells were lysed via sonication and then spun down at 4 °C at 12,000
419 RPM for 30 minutes. The supernatant was further processed using a 1 mL HisTrap HP column
420 (Cytiva), prepared according to the manufacturer's directions, washed with wash buffer (20 mM
421 Tris-HCl, 500 mM NaCl, 30 mM imidazole, pH 7.4) and eluted with elution buffer (20 mM Tris-
422 HCl, 500 mM NaCl, 500 mM imidazole, pH 7.4). The concentration of the purified protein was
423 determined by Bradford assay with a BSA standard (57).
424
425 **Electrophoretic mobility shift assay (EMSA).** Labeled DNA was prepared using FAM
426 conjugated oligos (IDT) to amplify a portion of the *pfabHAF* region (see Table S4 for primers)
427 and the resulting amplicon was digested with *ndeI* and purified to produce FAM fragments either
428 with or without the *fapR* binding consensus sequence. Equimolar amounts of protein and DNA
429 were added to 10 µL reactions prepared using buffer as detailed in Schujman et al., 2003.
430 Briefly, the buffer consisted of 20 mM Tris-HCl (pH 8.0), 0.5 mM EDTA, 50 mM NaCl, 1 mM
431 DTT, 5 % glycerol. The reactions were incubated in the dark for 10 minutes at 37 °C before
432 addition of malonyl-CoA followed by an additional 10-minute incubation period under the same

433 conditions. The samples were loaded onto a pre-run 10 % non-denaturing acrylamide gel in 1x
434 TBE buffer. Electrophoresis was performed at 100 V and the gel was imaged using a Typhoon
435 FLA 7000 (GE Healthcare Life Sciences) and quantification was performed using Fiji (58).
436

437 **Fatty acid methyl esterase analysis (FAME)**

438 Freshly streaked strains were grown in LB medium overnight at 37 °C with shaking. The pre-
439 culture was then used to inoculate 100 mL of LB medium and grown at 37 °C with shaking until
440 0.4 OD_{600nm}. 20-30 mg of cells were harvested and stored at -80 °C. Sample preparation and
441 FAME direct analysis was performed by Microbial ID (Newark, DE). Reported values represent
442 the average and standard deviations of biological triplicates.
443

444 **Microscopic evaluation**

445 The indicated strains were grown until ~0.4 OD_{600nm} and spotted onto a slide containing a thin
446 pad prepared from 1% agarose. The cells were allowed to air-dry before application of a cover
447 slip. The cells were imaged at 100x magnification with immersion oil using an Olympus BX61
448 microscope and images were captured using a Cooke Sensicam camera. Cell lengths and widths
449 were determined using the Fiji (58) plugin, MicrobeJ (59). A minimum of 100 cell lengths and
450 widths were recorded for statistical analysis.
451

452 **Minimal inhibitory concentration (MIC) determination and fractional inhibitory**
453 **concentration index (FICI) calculation**

454 An MIC for each indicated drug was first identified as the drug concentration where a WT strain
455 did not reach ~0.2 OD_{600nm} following 10 hours of treatment. The MIC of drugs individually are

456 as follows: 1000 µg/mL bacitracin, 1.28 µg/mL cefuroxime, 5 µg/mL cerulenin, 1 µg/mL
457 chloramphenicol, 50 µg/mL D-cycloserine, 50 µg/mL fosfomycin, 200 µg/mL nisin, 0.75 µg/mL
458 triclosan, 0.15 µg/mL vancomycin. The index (FICI) for drug combinations was calculated as
459 follows with FIC = $(A/MIC_A) + (B/MIC_B)$ where A and B are the MIC of each antibiotic in
460 combination and MIC_A and MIC_B are the MIC of each antibiotic individually. The FICI of < 0.5
461 is considered as synergistic, 0.5-4 as additive and >4 as antagonistic (60).
462

463 **ACKNOWLEDGEMENTS**

464 This work was supported by the National Institutes of Health (grant R35GM122461 to JDH).
465 The funders had no role in study design, data collection and analysis, decision to publish, or
466 preparation of the manuscript. We acknowledge Heng Zhao for guidance with the reconstruction
467 of *fapR** suppressor via CRISPR-cas9 mutagenesis. We thank the Angert lab for use of their
468 light microscope and Yesha Patel, Ankita Sachla, and Tobias Dörr for helpful comments.
469
470

471 **References**

472 1. Egan AJF, Errington J, Vollmer W. 2020. Regulation of peptidoglycan synthesis and remodelling.
473 Nat Rev Microbiol 18:446-460.
474 2. Zhao H, Patel V, Helmann JD, Dörr T. 2017. Don't let sleeping dogmas lie: new views of
475 peptidoglycan synthesis and its regulation. Mol Microbiol 106:847-860.
476 3. Nguyen LT, Gumbart JC, Beeby M, Jensen GJ. 2015. Coarse-grained simulations of bacterial cell
477 wall growth reveal that local coordination alone can be sufficient to maintain rod shape. Proc
478 Natl Acad Sci U S A 112:E3689-98.

479 4. Barreteau H, Kovac A, Boniface A, Sova M, Gobec S, Blanot D. 2008. Cytoplasmic steps of
480 peptidoglycan biosynthesis. FEMS Microbiol Rev 32:168-207.
481 5. Claessen D, Emmins R, Hamoen LW, Daniel RA, Errington J, Edwards DH. 2008. Control of the cell
482 elongation-division cycle by shuttling of PBP1 protein in *Bacillus subtilis*. Mol Microbiol 68:1029-
483 46.
484 6. Garner EC, Bernard R, Wang W, Zhuang X, Rudner DZ, Mitchison T. 2011. Coupled,
485 circumferential motions of the cell wall synthesis machinery and MreB filaments in *B. subtilis*.
486 Science 333:222-5.
487 7. Domínguez-Escobar J, Chastanet A, Crevenna AH, Fromion V, Wedlich-Söldner R, Carballido-
488 López R. 2011. Processive movement of MreB-associated cell wall biosynthetic complexes in
489 bacteria. Science 333:225-8.
490 8. Vigouroux A, Cordier B, Aristov A, Alvarez L, Özbaykal G, Chaze T, Oldewurtel ER, Matondo M,
491 Cava F, Bikard D, van Teeffelen S. 2020. Class-A penicillin binding proteins do not contribute to
492 cell shape but repair cell-wall defects. Elife 9.
493 9. Straume D, Piechowiak KW, Kjos M, Håvarstein LS. 2021. Class A PBPs: It is time to rethink
494 traditional paradigms. Mol Microbiol 116:41-52.
495 10. Dion MF, Kapoor M, Sun Y, Wilson S, Ryan J, Vigouroux A, van Teeffelen S, Oldenbourg R, Garner
496 EC. 2019. *Bacillus subtilis* cell diameter is determined by the opposing actions of two distinct cell
497 wall synthetic systems. Nat Microbiol 4:1294-1305.
498 11. Helmann JD. 2016. *Bacillus subtilis* extracytoplasmic function (ECF) sigma factors and defense of
499 the cell envelope. Curr Opin Microbiol 30:122-132.
500 12. Eiamphungporn W, Helmann JD. 2008. The *Bacillus subtilis* sigma(M) regulon and its
501 contribution to cell envelope stress responses. Mol Microbiol 67:830-48.

502 13. Mascher T, Hachmann AB, Helmann JD. 2007. Regulatory overlap and functional redundancy
503 among *Bacillus subtilis* extracytoplasmic function sigma factors. J Bacteriol 189:6919-27.
504 14. Meeske AJ, Riley EP, Robins WP, Uehara T, Mekalanos JJ, Kahne D, Walker S, Kruse AC,
505 Bernhardt TG, Rudner DZ. 2016. SEDS proteins are a widespread family of bacterial cell wall
506 polymerases. Nature 537:634-638.
507 15. McPherson DC, Popham DL. 2003. Peptidoglycan synthesis in the absence of class A penicillin-
508 binding proteins in *Bacillus subtilis*. J Bacteriol 185:1423-31.
509 16. Sjodt M, Rohs PDA, Gilman MSA, Erlandson SC, Zheng S, Green AG, Brock KP, Taguchi A, Kahne
510 D, Walker S, Marks DS, Rudner DZ, Bernhardt TG, Kruse AC. 2020. Structural coordination of
511 polymerization and crosslinking by a SEDS-bPBP peptidoglycan synthase complex. Nat Microbiol
512 5:813-820.
513 17. Emami K, Guyet A, Kawai Y, Devi J, Wu LJ, Allenby N, Daniel RA, Errington J. 2017. RodA as the
514 missing glycosyltransferase in *Bacillus subtilis* and antibiotic discovery for the peptidoglycan
515 polymerase pathway. Nat Microbiol 2:16253.
516 18. Patel Y, Zhao H, Helmann JD. 2020. A regulatory pathway that selectively up-regulates
517 elongasome function in the absence of class A PBPs. Elife 9.
518 19. Heinrich J, Lundén T, Kontinen VP, Wiegert T. 2008. The *Bacillus subtilis* ABC transporter EcsAB
519 influences intramembrane proteolysis through RasP. Microbiology (Reading) 154:1989-1997.
520 20. Hastie JL, Williams KB, Ellermeier CD. 2013. The activity of σ^V, an extracytoplasmic function σ
521 factor of *Bacillus subtilis*, is controlled by regulated proteolysis of the anti-σ factor RsiV. J
522 Bacteriol 195:3135-44.
523 21. Hastie JL, Williams KB, Sepúlveda C, Houtman JC, Forest KT, Ellermeier CD. 2014. Evidence of a
524 bacterial receptor for lysozyme: binding of lysozyme to the anti-σ factor RsiV controls activation
525 of the ECF σ factor $\sigma^{V.}$ PLoS Genet 10:e1004643.

526 22. Parrell D, Zhang Y, Olenic S, Kroos L. 2017. *Bacillus subtilis* Intramembrane Protease RasP
527 Activity in *Escherichia coli* and In Vitro. J Bacteriol 199.
528 23. Liu TY, Chu SH, Hu YN, Wang JJ, Shaw GC. 2017. Genetic evidence that multiple proteases are
529 involved in modulation of heat-induced activation of the sigma factor SigI in *Bacillus subtilis*.
530 FEMS Microbiol Lett 364.
531 24. Zuber U, Drzewiecki K, Hecker M. 2001. Putative sigma factor SigI (YkoZ) of *Bacillus subtilis* is
532 induced by heat shock. J Bacteriol 183:1472-5.
533 25. Tesson B, Dajkovic A, Keary R, Marlière C, Dupont-Gillain CC, Carballido-López R. 2022.
534 Magnesium rescues the morphology of *Bacillus subtilis mreB* mutants through its inhibitory
535 effect on peptidoglycan hydrolases. Sci Rep 12:1137.
536 26. Tong L. 2005. Acetyl-coenzyme A carboxylase: crucial metabolic enzyme and attractive target for
537 drug discovery. Cell Mol Life Sci 62:1784-803.
538 27. Schujman GE, Paoletti L, Grossman AD, de Mendoza D. 2003. FapR, a bacterial transcription
539 factor involved in global regulation of membrane lipid biosynthesis. Dev Cell 4:663-72.
540 28. Schujman GE, Guerin M, Buschiazzo A, Schaeffer F, Llarrull LI, Reh G, Vila AJ, Alzari PM, de
541 Mendoza D. 2006. Structural basis of lipid biosynthesis regulation in Gram-positive bacteria.
542 Embo J 25:4074-83.
543 29. Strahl H, Bürmann F, Hamoen LW. 2014. The actin homologue MreB organizes the bacterial cell
544 membrane. Nat Commun 5:3442.
545 30. Kingston AW, Subramanian C, Rock CO, Helmann JD. 2011. A σ^W-dependent stress response in
546 *Bacillus subtilis* that reduces membrane fluidity. Mol Microbiol 81:69-79.
547 31. Moche M, Schneider G, Edwards P, Dehesh K, Lindqvist Y. 1999. Structure of the complex
548 between the antibiotic cerulenin and its target, beta-ketoacyl-acyl carrier protein synthase. J
549 Biol Chem 274:6031-4.

550 32. Campbell JW, Cronan JE, Jr. 2001. Bacterial fatty acid biosynthesis: targets for antibacterial drug
551 discovery. Annu Rev Microbiol 55:305-32.
552 33. Zhang YM, White SW, Rock CO. 2006. Inhibiting bacterial fatty acid synthesis. J Biol Chem
553 281:17541-4.
554 34. Hutter B, Schaab C, Albrecht S, Borgmann M, Brunner NA, Freiberg C, Ziegelbauer K, Rock CO,
555 Ivanov I, Loferer H. 2004. Prediction of mechanisms of action of antibacterial compounds by
556 gene expression profiling. Antimicrob Agents Chemother 48:2838-44.
557 35. Wille W, Eisenstadt E, Willecke K. 1975. Inhibition of de novo fatty acid synthesis by the
558 antibiotic cerulenin in *Bacillus subtilis*: effects on citrate-Mg^{2+} transport and synthesis of
559 macromolecules. Antimicrob Agents Chemother 8:231-7.
560 36. Vadia S, Tse JL, Lucena R, Yang Z, Kellogg DR, Wang JD, Levin PA. 2017. Fatty Acid Availability
561 Sets Cell Envelope Capacity and Dictates Microbial Cell Size. Curr Biol 27:1757-1767.e5.
562 37. Pulschen AA, Sastre DE, Machinandiarena F, Crotta Asis A, Albanesi D, de Mendoza D, Gueiros-
563 Filho FJ. 2017. The stringent response plays a key role in *Bacillus subtilis* survival of fatty acid
564 starvation. Mol Microbiol 103:698-712.
565 38. Paoletti L, Lu YJ, Schujman GE, de Mendoza D, Rock CO. 2007. Coupling of fatty acid and
566 phospholipid synthesis in *Bacillus subtilis*. J Bacteriol 189:5816-24.
567 39. Machinandiarena F, Nakamatsu L, Schujman GE, de Mendoza D, Albanesi D. 2020. Revisiting the
568 coupling of fatty acid to phospholipid synthesis in bacteria with FapR regulation. Mol Microbiol
569 114:653-663.
570 40. Winkler WC, Nahvi A, Roth A, Collins JA, Breaker RR. 2004. Control of gene expression by a
571 natural metabolite-responsive ribozyme. Nature 428:281-6.

572 41. Patel V, Wu Q, Chandrangsu P, Helmann JD. 2018. A metabolic checkpoint protein GlmR is
573 important for diverting carbon into peptidoglycan biosynthesis in *Bacillus subtilis*. PLoS Genet
574 14:e1007689.
575 42. Thomanek N, Arends J, Lindemann C, Barkovits K, Meyer HE, Marcus K, Narberhaus F. 2018.
576 Intricate Crosstalk Between Lipopolysaccharide, Phospholipid and Fatty Acid Metabolism in
577 Escherichia coli Modulates Proteolysis of LpxC. Front Microbiol 9:3285.
578 43. May KL, Silhavy TJ. 2018. The *Escherichia coli* Phospholipase PldA Regulates Outer Membrane
579 Homeostasis via Lipid Signaling. mBio 9.
580 44. Errington J, Mickiewicz K, Kawai Y, Wu LJ. 2016. L-form bacteria, chronic diseases and the origins
581 of life. Philos Trans R Soc Lond B Biol Sci 371.
582 45. Mercier R, Kawai Y, Errington J. 2013. Excess membrane synthesis drives a primitive mode of cell
583 proliferation. Cell 152:997-1007.
584 46. Siddiqui RA, Hoischen C, Holst O, Heinze I, Schlott B, Gumpert J, Diekmann S, Grosse F, Platzer
585 M. 2006. The analysis of cell division and cell wall synthesis genes reveals mutationally
586 inactivated *ftsQ* and *mraY* in a protoplast-type L-form of *Escherichia coli*. FEMS Microbiol Lett
587 258:305-11.
588 47. Niederman RA. 2013. Membrane development in purple photosynthetic bacteria in response to
589 alterations in light intensity and oxygen tension. Photosynth Res 116:333-48.
590 48. Yao Z, Davis RM, Kishony R, Kahne D, Ruiz N. 2012. Regulation of cell size in response to nutrient
591 availability by fatty acid biosynthesis in *Escherichia coli.* Proc Natl Acad Sci U S A 109:E2561-8.
592 49. Tödter D, Gunka K, Stülke J. 2017. The Highly Conserved Asp23 Family Protein YqhY Plays a Role
593 in Lipid Biosynthesis in *Bacillus subtilis*. Front Microbiol 8:883.
594 50. Willdigg JR, Helmann JD. 2021. Mini Review: Bacterial Membrane Composition and Its
595 Modulation in Response to Stress. Frontiers in Molecular Biosciences 8.

596 51. Kurita K, Kato F, Shiomi D. 2020. Alteration of Membrane Fluidity or Phospholipid Composition
597 Perturbs Rotation of MreB Complexes in *Escherichia coli*. Front Mol Biosci 7:582660.
598 52. van Teeffelen S, Wang S, Furchtgott L, Huang KC, Wingreen NS, Shaevitz JW, Gitai Z. 2011. The
599 bacterial actin MreB rotates, and rotation depends on cell-wall assembly. Proc Natl Acad Sci U S
600 A 108:15822-7.
601 53. Zielińska A, Savietto A, de Sousa Borges A, Martinez D, Berbon M, Roelofsen JR, Hartman AM, de
602 Boer R, Van der Klei IJ, Hirsch AK, Habenstein B, Bramkamp M, Scheffers DJ. 2020. Flotillin-
603 mediated membrane fluidity controls peptidoglycan synthesis and MreB movement. Elife 9.
604 54. Kearns DB, Chu F, Branda SS, Kolter R, Losick R. 2005. A master regulator for biofilm formation
605 by *Bacillus subtilis*. Mol Microbiol 55:739-49.
606 55. Altenbuchner J. 2016. Editing of the *Bacillus subtilis* Genome by the CRISPR-Cas9 System. Appl
607 Environ Microbiol 82:5421-7.
608 56. Quisel JD, Burkholder WF, Grossman AD. 2001. In vivo effects of sporulation kinases on mutant
609 Spo0A proteins in *Bacillus subtilis*. J Bacteriol 183:6573-8.
610 57. Bradford MM. 1976. A rapid and sensitive method for the quantitation of microgram quantities
611 of protein utilizing the principle of protein-dye binding. Anal Biochem 72:248-54.
612 58. Schindelin J, Arganda-Carreras I, Frise E, Kaynig V, Longair M, Pietzsch T, Preibisch S, Rueden C,
613 Saalfeld S, Schmid B, Tinevez JY, White DJ, Hartenstein V, Eliceiri K, Tomancak P, Cardona A.
614 2012. Fiji: an open-source platform for biological-image analysis. Nat Methods 9:676-82.
615 59. Ducret A, Quardokus EM, Brun YV. 2016. MicrobeJ, a tool for high throughput bacterial cell
616 detection and quantitative analysis. Nat Microbiol 1:16077.
617 60. Odds FC. 2003. Synergy, antagonism, and what the chequerboard puts between them. J
618 Antimicrob Chemother 52:1.
619

s

Table 1. **Spontaneous suppressor mutations recovered in PG-limited cells.** Mutants of the *ecsA ponA* and *rasP ponA* parent strains were selected that were able to grow in LB medium in the absence of magnesium supplementation. Each suppressor strain contained a single point mutation identified via whole genome re-sequencing. The genome position was determined via comparison to the *B. subtills* reference genome NC_000964.3.

Isolate	Strain Background	Gene	Genome Position	Nucleotide Change	Mutation
HB23854	*ecsA ponA*	*fapR*	1662276	A --> G	Δ24 bp deletion in CDC/ I104V
HB23855	*ecsA ponA*	*fapR*	1662301	C --> T	A112V
HB23856	*ecsA ponA*	*accA*	2988324	C --> A	G129W
HB23857	*ecsA ponA*	*accA*	2988009	A --> G	T234R
HB23860	*ecsA ponA*	*accB*	2532222	T --> C	SNP between promoter and RBS
HB23885	*rasP ponA*	*fapR*	1662190	T --> A	175N
HB23874	*rasP ponA*	*accA*	2988055	G --> T	N218K
HB23875	*rasP ponA*	*accC*	2531202	T --> C	R169G
HB23883	*rasP ponA*	*accC*	2531393	G --> A	P105L
HB23877	*rasP ponA*	*accD*	2989081	G --> A	T162M
HB23879	*rasP ponA*	*accD*	2989654	T --> deletion	deletion in promoter

629

630 **Table 2. FICI values of cerulenin in combination with selected cell wall synthesis targeting**

631 **antibiotics.** An MIC was defined as having and OD_{600} below 0.2 after 10 hours of treatment.

632 Susceptibility was defined as follows: < 0.5 synergistic, 0.5-4 indifferent, > 5 antagonistic.

633

Strain	Compound A	Compound B	FIC	Susceptibility Pattern
WT	Bacitracin	Cerulenin	5	Antagonistic
	Bacitracin	Triclosan	1.03	Indifferent
	Bacitracin	Chloramphenicol	1	Indifferent
	Cefuroxime	Cerulenin	2.5	Indifferent
	D-Cycloserine	Cerulenin	2	Indifferent
	Fosfomycin	Cerulenin	3	Indifferent
	Nisin	Cerulenin	2	Indifferent
	Vancomycin	Cerulenin	2	Indifferent
sigI	Cefuroxime	Cerulenin	16	Antagonistic

634

635

636

FIGURE LEGENDS

Figure 1. **FAS suppressor mutations rescue cells with lethal PG synthesis defects.** (A) The FapR* 24-nucleotide deletion occurs in the thioesterase-like, malonyl-CoA binding domain of the protein. Asterisks indicate residues important for coordinating the interaction between FapR and malonyl-CoA. (B) *fapR** rescues viability of *ecsA ponA*, *rasP ponA*, and *sigI ponA* cells in LB medium in the absence of magnesium supplementation. (C) Deletion of FapR does not rescue viability of a *sigI ponA* mutant grown in LB medium in the absence of magnesium supplementation. (D) *fapR** is dominant in a merodiploid strain expressing at locus *fapR*.

Figure 2. ***fapR**** **decreases the expression of FAS genes.** (A) Gene expression from candidate genes in the *fapR* regulon (*fabF, fapR and fabHA)* is decreased in a *fapR** mutant. The x-axis indicates candidate genes detected, and the legend indicates strain genotypes. ND indicates a lack of *fapR* gene expression in a *fapR* null background. Gene expression values ($2^{-\Delta ct}$) were normalized to *gyrA* and plotted. A one-way ANOVA with a Tukey test for multiple comparisons was performed. P-value cutoff (*) < 0.05.

Figure 3. **FapR* exhibits altered interactions with malonyl-CoA.** (A) Gel shift assay where a FapR-DNA complex was titrated with increasing concentrations of malonyl-CoA. The lower DNA bands serve both as a loading control and control for protein interaction specificity as it does not contain the FapR recognized inverted repeat and is therefore not expected to shift upon addition of FapR. The ratio of protein-DNA was kept constant for all conditions. (B) Gel shift assay where FapR*-DNA complex was titrated with increasing concentrations of malonyl-CoA

under same conditions as above. (C) The fraction unbound DNA under different concentrations of malonyl-CoA was determined by calculating the ratio of intensity of the shifted protein-DNA band to the unshifted control band. All values were normalized to 1. N=3 representative trials.

Figure 4. **Increased membrane fluidity can restore viability to PG-limited cells.** (A) A representative zone of growth obtained following application of 10% BnoH to a plate inoculated with the indicated strains. *sigI ponA* and *sigW sigI ponA* have a higher propensity to form suppressor mutation on LB medium in the absence of high concentrations of magnesium compared to that of *rasP ponA* as seen by the isolated colonies on the plate. (B) Treatment with 10% BnOH creates a zone of growth when applied to *sigI ponA* cells grown on LB medium in the absence of high concentrations of magnesium but fails to rescue *rasP ponA*. A one-way ANOVA with Tukey test for multiple comparisons was performed. P-value > 0.05. The size of the filter disc (6mm) was subtracted from the zone of growth values.

Figure 5. ***fapR* cells exhibit increased sensitivity to conditions that increase membrane fluidity.*** (A) FapR* cells demonstrate an increased sensitivity to Triton X-100. P-value cutoff (*) < 0.05. The size of the filter disc (6mm) was subtracted from all zone of inhibition values. (B) The *fapR** cells sensitized to heat with a *sigI* null deletion experience increased sensitivity to heat (56 °C). (C) The *fapR** mediated rescue is lost in the *ecsA ponA*, *rasP ponA*, and *sigI ponA* at increased temperatures.

Figure 6. ***fapR* sensitizes cells to the FAS-inhibiting effects of cerulenin***. (A) *fapR** exhibits an increased sensitivity to cerulenin compared to WT and *fapR* null cells, but not to triclosan. No

683 comparison was performed between antibiotic groups. A one-way ANOVA with Tukey test for
684 multiple comparisons was performed for each antibiotic group. P-value cutoff (***) < 0.0002.
685 The size of the filter disc (6mm) was subtracted from the zone of inhibition values.
686
687 Figure 7. **Chemical inhibition of FAS by cerulenin is sufficient to rescue the *rasP ponA***
688 **strain.** (A) Increasing concentrations of cerulenin rescue growth of a *rasP ponA* strain grown in
689 LB medium in the absence of high concentrations of magnesium.
690

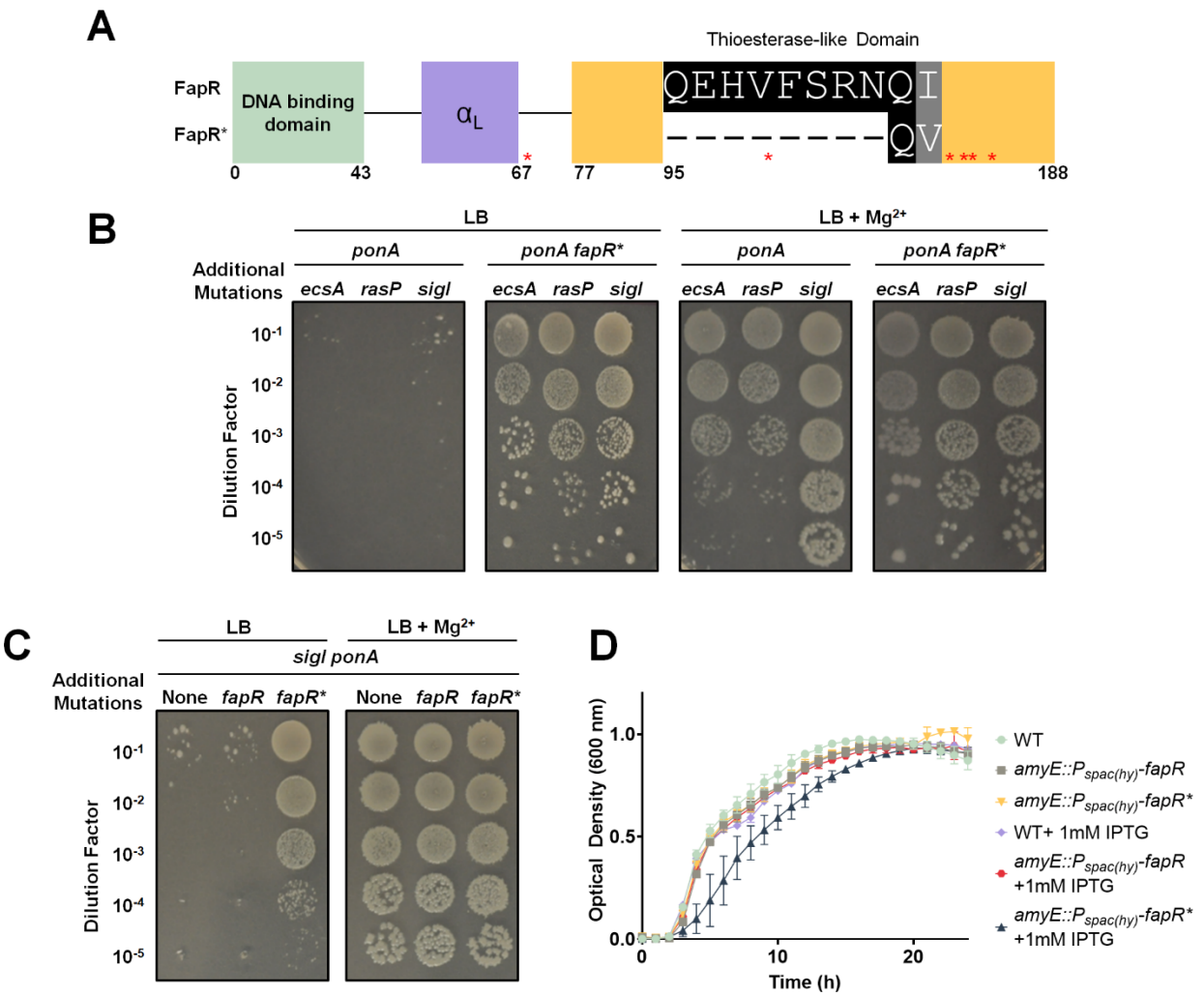

Figure 1. **FAS suppressor mutations rescue cells with lethal PG synthesis defects.** (A) The FapR* 24-nucleotide deletion occurs in the thioesterase-like, malonyl-CoA binding domain of the protein. Asterisks indicate residues important for coordinating the interaction between FapR and malonyl-CoA. (B) *fapR** rescues viability of *ecsA ponA*, *rasP ponA*, and *sigI ponA* cells in LB medium in the absence of magnesium supplementation. (C) Deletion of FapR does not rescue viability of a *sigI ponA* mutant grown in LB medium in the absence of magnesium supplementation. (D) *fapR** is dominant in a merodiploid strain expressing at locus *fapR*.

10

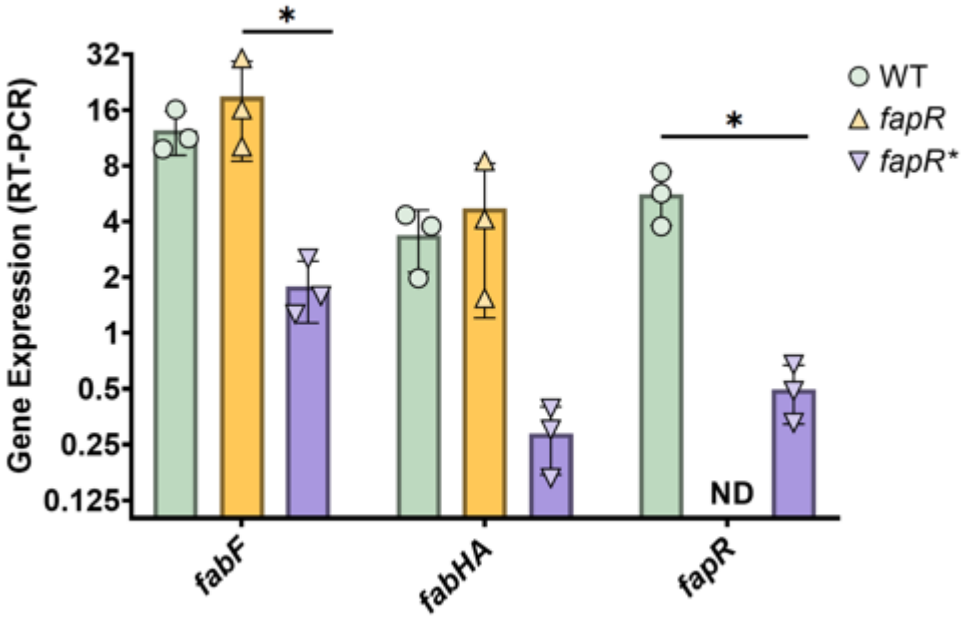

11

12

13 Figure 2. ***fapR* decreases the expression of FAS genes.*** (A) Gene expression from candidate
14 genes in the *fapR* regulon (*fabF, fapR and fabHA)* is decreased in a *fapR** mutant. The x-axis
15 indicates candidate genes detected, and the legend indicates strain genotypes. ND indicates a
16 lack of *fapR* gene expression in a *fapR* null background. Gene expression values ($2^{-\Delta ct}$) were
17 normalized to *gyrA* and plotted. A one-way ANOVA with a Tukey test for multiple comparisons
18 was performed. P-value cutoff (*) < 0.05.

19

20

21

22

23

24

25

26

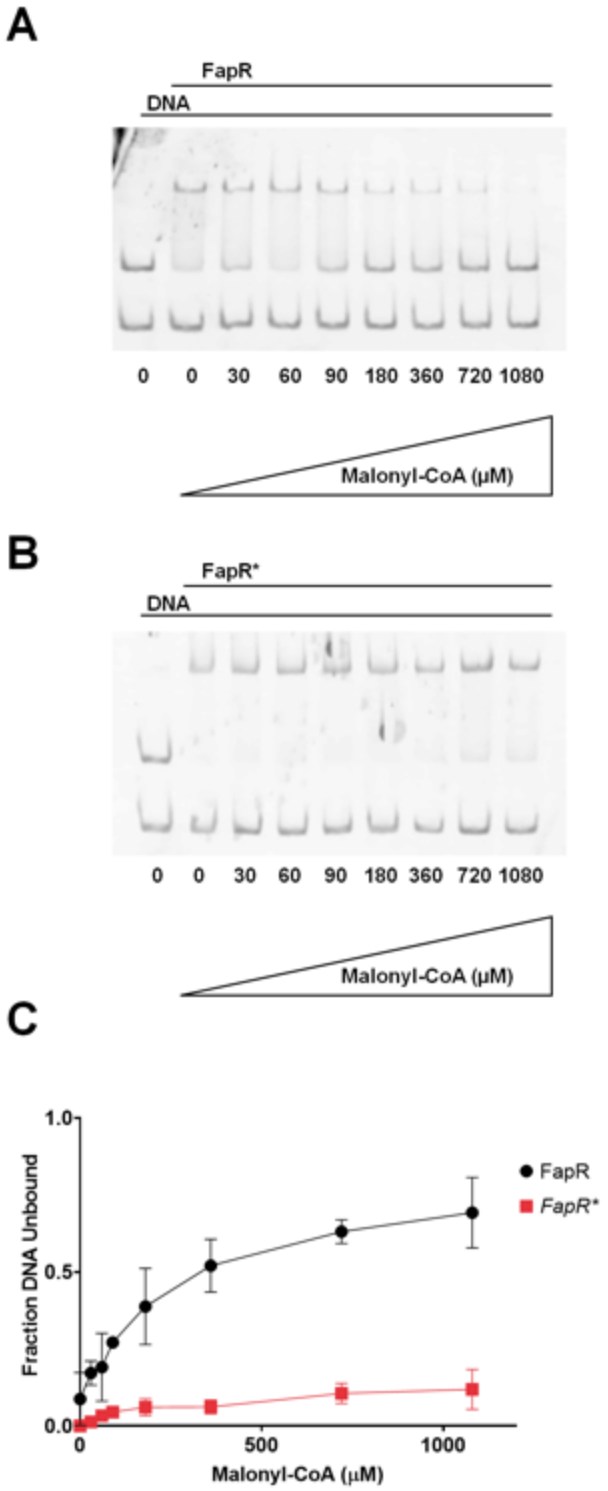

Figure 3. **FapR* exhibits altered interactions with malonyl-CoA.** (A) Gel shift assay where a FapR-DNA complex was titrated with increasing concentrations of malonyl-CoA. The lower DNA bands serve both as a loading control and control for protein interaction specificity as it

31 does not contain the FapR recognized inverted repeat and is therefore not expected to shift upon
32 addition of FapR. The ratio of protein-DNA was kept constant for all conditions. (B) Gel shift
33 assay where FapR*-DNA complex was titrated with increasing concentrations of malonyl-CoA
34 under same conditions as above. (C) The fraction unbound DNA under different concentrations
35 of malonyl-CoA was determined by calculating the ratio of intensity of the shifted protein-DNA
36 band to the unshifted control band. All values were normalized to 1. N=3 representative trials.
37

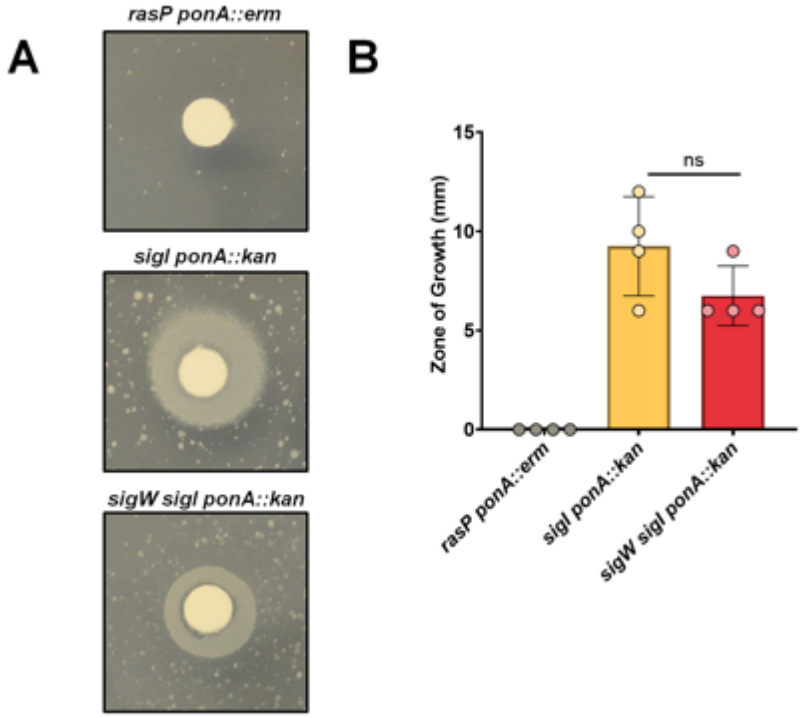

38
39 Figure 4. **Increased membrane fluidity can restore viability to PG-limited cells.** (A) A
40 representative zone of growth obtained following application of 10% BnoH to a plate inoculated
41 with the indicated strains. *sigI ponA* and *sigW sigI ponA* have a higher propensity to form
42 suppressor mutation on LB medium in the absence of high concentrations of magnesium
43 compared to that of *rasP ponA* as seen by the isolated colonies on the plate. (B) Treatment with
44 10% BnOH creates a zone of growth when applied to *sigI ponA* cells grown on LB medium in
45 the absence of high concentrations of magnesium but fails to rescue *rasP ponA*. A one-way
46 ANOVA with Tukey test for multiple comparisons was performed. P-value > 0.05. The size of
47 the filter disc (6mm) was subtracted from the zone of growth values.
48

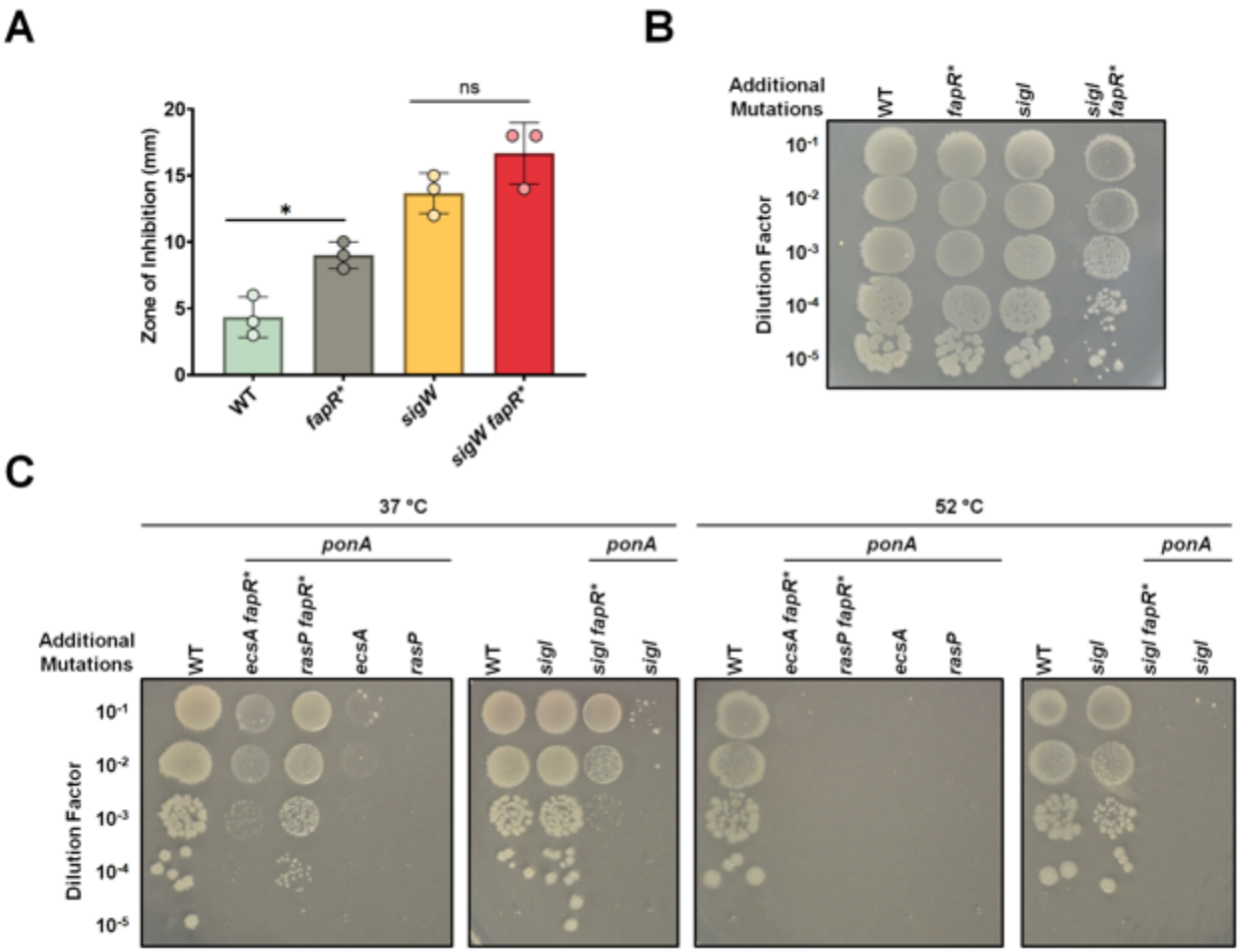

Figure 5. ***fapR* cells exhibit increased sensitivity to conditions that increase membrane fluidity.*** (A) FapR* cells demonstrate an increased sensitivity to Triton X-100. P-value cutoff (*) < 0.05. The size of the filter disc (6mm) was subtracted from all zone of inhibition values. (B) The *fapR** cells sensitized to heat with a *sigI* null deletion experience increased sensitivity to heat (56 °C). (C) The *fapR** mediated rescue is lost in the *ecsA ponA*, *rasP ponA*, and *sigI ponA* at increased temperatures.

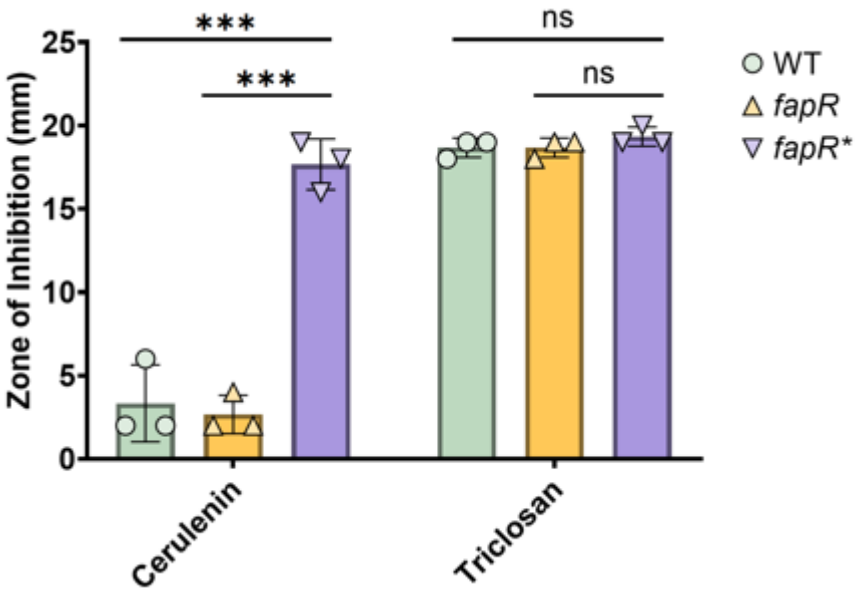

63

64

65 Figure 6. ***fapR* sensitizes cells to the FAS-inhibiting effects of cerulenin***. (A) *fapR** exhibits
66 an increased sensitivity to cerulenin compared to WT and *fapR* null cells, but not to triclosan. No
67 comparison was performed between antibiotic groups. A one-way ANOVA with Tukey test for
68 multiple comparisons was performed for each antibiotic group. P-value cutoff (***) < 0.0002.
69 The size of the filter disc (6mm) was subtracted from the zone of inhibition values.

70

71

72

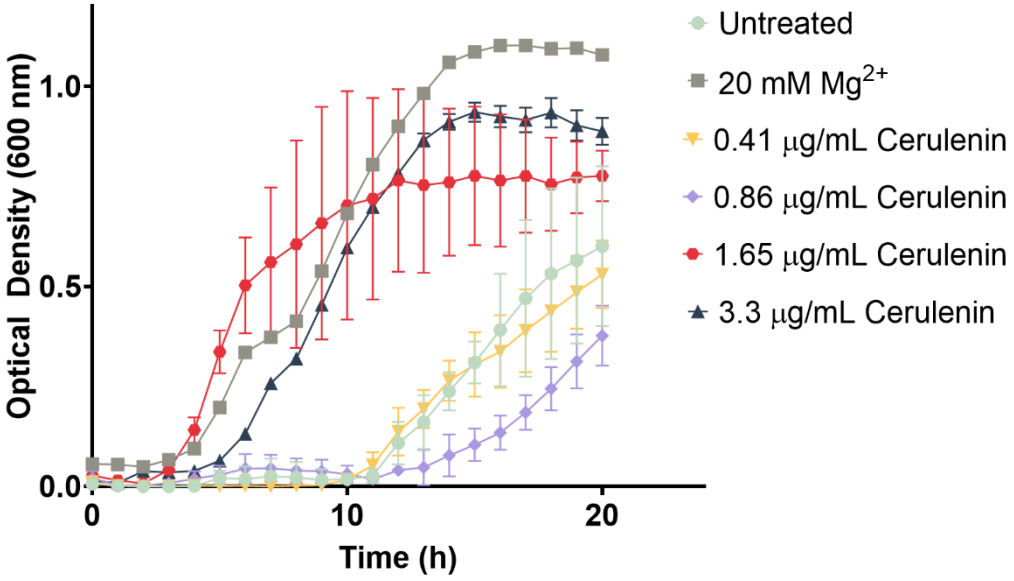

Figure 7. **Chemical inhibition of FAS by cerulenin is sufficient to rescue the *rasP ponA* strain.** (A) Increasing concentrations of cerulenin rescue growth of a *rasP ponA* strain grown in LB medium in the absence of high concentrations of magnesium.